




InP integrated optical frequency comb generator using an amplified recirculating loop

EUAN J. TOUGH,^{1,*}  MARTYN J. FICE,¹ GUILLERMO CARPINTERO,²
CYRIL C. RENAUD,¹ ALWYN J. SEEDS,¹
AND KATARZYNA BALAKIER^{1,3}

¹Department of Electronic and Electrical Engineering, University College London, London, UK

²Department of Electronic Technology, Universidad Carlos III de Madrid, Madrid, Spain

³currently with European Space Agency (ESA/ECSAT), Harwell, UK

*uceetou@ucl.ac.uk

Abstract: A novel realisation of photonically integrated optical frequency comb generation is demonstrated on indium phosphide (InP) using a generic foundry platform. The architecture, based on the amplified recirculating loop technique, consists of cascaded electro-optic phase modulators embedded within a short waveguide loop. While an injected continuous wave laser signal is recirculated by the loop, the modulators are driven with a modulation frequency corresponding to the round-trip loop length frequency. This results in many phase coherent, evenly spaced optical comb lines being generated. The choice of InP as an integration platform allows immediate optical amplification of the modulated signal by embedded semiconductor optical amplifiers, enabling loop losses to be compensated and expanding the comb across broad optical bandwidths. This approach reduces the requirement for external, high-power optical amplifiers, improving the compactness and power efficiency of the full system. The system was modelled to identify off-resonance behaviour, outlining limits in matching both the modulation frequency and seed laser frequency to the round-trip loop frequency for optimal comb line generation to be achieved. The experimental device occupied a fraction of the 6 x 2 mm² InP chip and operated at round-trip loop frequencies of 6.71 GHz to produce 59 comb lines within a 20 dB power envelope. All comb lines exhibited strong phase coherence as characterised by low composite phase noise measurements of -105 dBc/Hz at 100 kHz. A second device is also presented with a shorter loop length operating at ~10 GHz which generated 57 comb lines. Both loop configurations included short waveguide phase shifters providing a degree of tunability of the free spectral range with a tuning range of 150 MHz for small injection currents of < 2.5 mA.

Published by Optica Publishing Group under the terms of the [Creative Commons Attribution 4.0 License](https://creativecommons.org/licenses/by/4.0/). Further distribution of this work must maintain attribution to the author(s) and the published article's title, journal citation, and DOI.

1. Introduction

Optical frequency comb generators (OFCGs) are optical sources capable of generating multiple phase coherent optical tones, evenly spaced across broad optical bandwidths, and have rapidly become fundamental building blocks in many photonic systems across a range of disciplines, including metrology and precision timekeeping [1], microwave photonics [2], spectroscopy [3,4], LIDAR [5] and high-speed optical communications [6]. The characteristics of the comb spectrum desired by each application can vary drastically, leading to the development of a diverse range of OFCG techniques capable of generating a variety of comb spectrum outputs. Comb generation techniques can therefore be selected and tailored to suit the particular criteria required to meet the performance level of the specific application. For instance, optical communication systems that utilise wavelength division multiplexing (WDM) demand broad comb spans with accurate channel spacing and good spectral flatness, which can be attained through integrated

mode-locked laser (MLL) techniques [7], whilst spectroscopy applications often prioritise tunability of both the central wavelength and comb line spacing, which are features most easily attained using comb techniques based on electro-optic (EO) modulation [8]. Irrespective of the application choice, OFCG techniques that offer low cost fabrication, occupy a compact footprint and operate with low power consumption are always advantageous, which has led to considerable exploration into the development of miniaturised comb generation technologies using photonically integrated platforms. The advent of these integrated technologies has enabled vast potential for the demonstration of applications that are reliant upon low size, weight and power consumption (SWaP) characteristics for OFCG solutions, such as performing frequency up/down conversion through multi-band local oscillators in communication satellites [9,10] or through the deployment of advanced driver assistance systems in the automotive industry with on-board LIDAR and photonic sensing [5,11].

The availability of foundry fabrication techniques has greatly expanded in the last decade, providing reliable fabrication capabilities for photonic integrated circuits (PICs) in large volumes by wafer scale manufacturing. The small footprint of PICs can be occupied by a high density of active and passive components to realise the monolithic integration of complex optical systems. Many established foundry platforms including indium phosphide (InP), thin film lithium niobate (TFLN), silicon on insulator (SoI) and silicon nitride (SiN) offer a sufficient component library and performance capabilities to enable different on-chip solutions for optical frequency comb (OFC) generation. Some examples of these integrated techniques include MLLs [12–16], gain-switched lasers [17,18], Kerr-comb microresonators [7] and EO based comb generators [19–25]. A summary of the state-of-the-art performance of these techniques has been outlined in Table 1 and a comprehensive review of their operating principles can be found in [26].

Integrated EO based comb generators are the focus of this work and have been demonstrated in numerous configurations utilising a combination of electro-optic phase modulators (EOPMs) or Mach-Zehnder modulators (MZMs) driven by radio frequency (RF) sources to generate sidebands that are evenly spaced by the modulation frequency [27]. As a result, the free spectral range (FSR) is often highly tunable and limited only by the bandwidth of the modulator, though the span of the generated comb is typically restricted to hundreds of GHz [28]. Through fine control of the driving characteristics and bias conditions of the EO modulators, comb spectra can be flattened to reduce the power difference between adjacent comb lines. MZM based comb generators on InP have generated upwards of 20 comb lines equally spaced at FSRs in the tens of GHz range and when driven in push-pull configurations, flat comb spectra can be achieved [19]. By linearly cascading multiple EO modulators, combs spans can typically be increased or the comb spectra can be flattened, depending on the configuration of cascaded EO modulators used. The number of cascaded components is usually limited to 2 or 3, bound by the increased complexity of additional driving electronics required to operate the device. Cascaded EO comb generators have been demonstrated with phase and intensity modulators on the InP platform to generate spans <50 GHz with comb spacing of <10 GHz [20,21] and similarly on the SoI platform with comb spans of <100 GHz and comb spacings of <10 GHz [22]. Recently, high-speed modulators on the TFLN platform have demonstrated the capability to generate broad optical comb spans with large FSRs of ~30 GHz. Single modulator designs have shown comb spans exceeding 1.2 THz [23] and cascaded MZM and EOPM configurations have demonstrated flat comb spectra spanning >400 GHz [24]. Further developments on TFLN have demonstrated EO modulators embedded within an ultralow loss, high Q-factor resonator, enabling multiple passes of a single EO modulator and utilising χ^2 non-linearities to vastly expand the comb span with over 900 comb lines spaced at around 10 GHz [25].

The approach outlined in this work involves the photonic integration of an EO based comb that utilises the amplified recirculating loop technique [29] of OFCG on InP. The paper will be comprised of the following sections. Section 2 will describe the OFCG operating principle

Table 1. Summary of state-of-the-art performance of integrated optical frequency comb generation techniques

OFCG Description	OFCG Technique	Platform	FSR ^a (GHz)	3-dB Bandwidth	OCNR ^b (dB)	Tunable
Passive Mode Locked Laser (Quantum Dot) [12]	MLL	Si	20	1.160 THz	20	No
Passive Mode Locked Laser (Quantum Dot) [13]	MLL	InP	92	1.469 THz	50	No
Passive Mode Locked Laser with Extended Cavity [14]	MLL	InP	50 - 450	< 840 GHz	22	Yes - FSR
Hybrid Mode Locked Laser with Extended Cavity [15]	MLL	InP/Si	20	360 GHz	25	No
Hybrid Mode Locked Laser with Extended Cavity [16]	MLL	InP/SiN	15.5	185 GHz	20	No
Gain Switched Laser [17]	DM ^c	InP	6.25	50 GHz	40	Yes - FSR
Externally Injected Gain-Switched Laser [18]	DM	InP	6 - 10	< 50 GHz	51	Yes - FSR
Kerr Comb Microresonator [7]	NLE ^d	SiN	100	6 THz	35	No
Dual Drive Mach-Zehnder Modulator [19]	EOM ^e	InP	10	290 GHz	25	Yes
Cascaded EO Modulators [20]	EOM	InP	4 - 10	< 50 GHz	25	Yes
Cascaded EO Modulators w/ Comb Line Multiplication [21]	EOM	InP	1-3	< 51 GHz	39	Yes
Cascaded EO Modulators [22]	EOM	SoI	< 10	90 GHz	20	Yes
Single EO Modulator [23]	EOM	TFLN	30	< 1.2 THz	35	Yes
Cascaded EO Modulators [24]	EOM	TFLN	31	400 GHz	35	Yes
Resonator Enhanced EO Modulator [25]	EOM/NLE	TFLN	10	750 GHz	40	No
Amplified Recirculating Loop w/ Cascaded EO Modulators (*this work)	EOM	InP	6.71	94 GHz	20	Yes

^aFree spectral range (FSR)

^bOptical carrier to noise ratio (OCNR)

^cDirect modulation (DM)

^dNon-linear effects (NLE)

^eElectro-optic modulation (EOM)

of the technique, including critical conditions that can be optimised to generate many optical comb lines, benefits and limitations of the integrated system, and a comparison to previously demonstrated fibre-based variations [30,31]. This will be followed by a comprehensive waveguide model of the integrated system with cascaded EOPMs embedded within the loop in Section 3, identifying the effect of varying critical parameters and the limitations in their specification. The photonic integrated device will be described in Section 4 including details of the PIC fabrication and a characterisations of active and passive components. The experimental setup for comb generation is also described. In Section 5 results are presented with comb spectra and phase noise measurements for the amplified recirculating loop device. In Section 6, a second device operating at a different round-trip loop frequency is then evaluated, concluding with a discussion of the tuning capabilities.

2. Comb operating principle

The operating principle of the amplified recirculating loop technique of OFC generation was first proposed by Ho and Kahn [29]. The system (Fig. 1) consists of a recirculating loop formed by a length of optical fibre with an EOPM and optical amplifier situated within it. A continuous-wave (CW) laser source couples into the loop providing an optical seed about which frequency shifted sidebands are generated. When the EOPM is driven with a sinusoidal modulation frequency, the sidebands are evenly spaced with a separation equal to the modulation frequency. The loop circulates the signal through the EOPM multiple times such that it experiences enhanced modulation on successive passes, expanding the comb by producing additional sidebands. Optical amplification within the loop enables round-trip loop losses to be compensated, maintaining sufficient optical power within the loop to be distributed to higher order sidebands, sustaining broad comb spans.

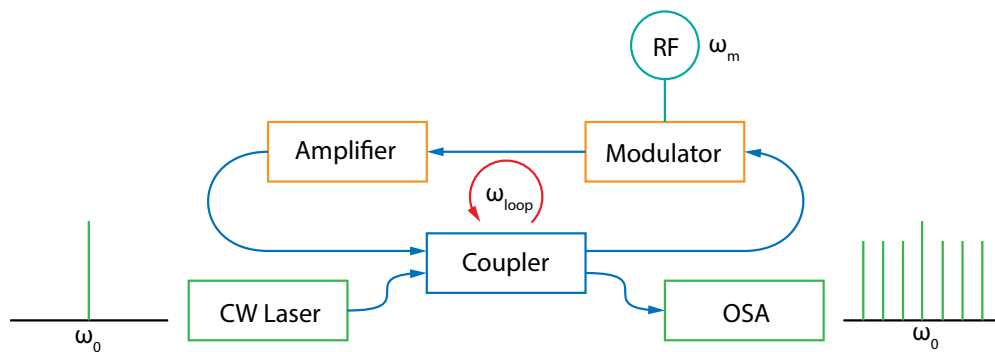


Fig. 1. Schematic of the amplified recirculating loop technique. A CW laser (ω_0) is coupled into the loop where sidebands are generated by the modulator with spacing equal to the applied RF frequency (ω_m). When ω_0 and ω_m are integer harmonics of the round-trip loop frequency (ω_{loop}), the recirculating mechanic is optimised to generate many phase coherent comb lines at the output optical spectrum analyser (OSA).

To ensure optimal operation with efficient enhancement of phase modulation on each recirculation, two conditions relating to the round-trip loop frequency (ω_{loop}), modulation frequency (ω_m) and carrier frequency (ω_0) need to be fulfilled:

$$\omega_m = p \cdot \omega_{loop}, \quad (1)$$

$$\omega_0 = q \cdot \omega_{loop}. \quad (2)$$

Condition 1 states that the EOPM must be driven with a ω_m that is an integer harmonic p of ω_{loop} , such that the phase modulated sidebands coincide with the cavity modes supported by the loop resonance. Similarly, condition 2 requires the frequency of the CW laser to be tuned to an integer harmonic q of ω_{loop} so that it is resonant with the cavity modes of the loop. The frequency of ω_{loop} is dependent upon the optical length of the loop, requiring the design of the loop length to be considered to ensure operation at appropriate FSR specifications.

Many examples of fibre-based systems utilising bulk components to configure the amplified recirculating loop have been demonstrated [30–32] and produced broad optical comb spans from a single EOPM. Often these demonstrations used recirculating loops with fibre lengths of around 20 m, producing narrow round-trip loop frequencies with cavity modes spaced by tens of MHz. Driving the system with a ω_m that was harmonic with the ω_{loop} enabled FSRs in the GHz range, desirable for telecom applications. An undesirable consequence from the length of fibre required to configure this design was that many cavity modes existed between the

modulated sidebands. With many closely spaced modes existing near the generated comb lines, these systems tended to suffer significantly from instability facilitated by temperature fluctuations that promoted mode hopping between adjacent modes. This meant the fibre-based systems were extremely sensitive to slight detuning in both ω_m , and to a lesser extent ω_0 [31]. Locking and feedback mechanisms could be implemented to suppress the instabilities, with methods that included injecting a broadened seed laser allowing many cavity modes to exist within a single comb line, or to create a feedback loop from a pick-off photodiode that controlled the bias of the EOPMs [29], or a piezo-electric fibre stretcher components embedded within the loop [31]. Additionally, the extended loop length succumbed to chromatic dispersion effects that distorted the even spacing of the cavity modes, resulting in misalignment of the higher order sidebands and the resonant modes of the loop that reduced the comb span. In [31] this was rectified with an appropriate length of dispersion compensated fibre incorporated within the loop. Using these techniques, stable comb generation of up to 3.8 THz span was demonstrated with tunable FSR of between 17.5 – 20 GHz and phase noise of -95 dBc/Hz at 100 kHz offset [31].

Using photonic integration techniques, the amplified recirculating loop was realised in this work as a monolithically integrated device with all components fabricated together on a single substrate. Integration has reduced the scale of the device significantly compared to equivalent fibre configurations, enabling a drastic improvement to the size, weight and power (SWAP) characteristics. The recirculating loop, now constructed from integrated optical waveguides, was fabricated including all necessary components with a total loop length of less than 12.5 mm, corresponding to round trip loop frequencies that directly support cavity modes spaced evenly by several to tens of GHz. This allowed the system to be driven with GHz modulation frequencies that were precisely equal to the cavity mode spacing of the loop rather than harmonics, removing the existence of closely spaced adjacent modes between comb lines and thus inherently improving the stability of the comb generation without additional feedback mechanisms. Furthermore, the small footprint of the PIC was easily temperature controlled to reduce thermal instabilities of the loop length that were prominently observed in the fibre-based loops.

The InP platform was chosen to provide direct amplification of the optical signal within the looped waveguide by semiconductor optical amplifiers (SOA). SOAs provided large gain bandwidths (up to 50 nm) within a 3 dB flatness that enabled the expansion of the comb over a wide span. Moreover, providing direct amplification on PIC removed the requirement for external optical amplification, thus reducing the entire system power consumption. The effect of using an SOA in an amplified recirculating loop has previously been demonstrated to cause only a small increase in the noise when compared to an erbium-doped fibre amplifier (EDFA) [33].

3. Simulation

A systems-based model was devised using VPI Photonics Design Suite to assess the photonic circuit representation of the amplified recirculating loop. Passive and active components were represented by parameter driven building blocks which are simulated by a hybrid time-and-frequency-domain modelling (TFDM) scheme. Passive waveguide circuit components were evaluated with an s-matrix approach using frequency-domain modelling where the behaviour of the waveguide is evaluated from the frequency-dependent propagation constant, $\beta_v(f)$, using the effective index model. After a second-order Taylor series expansion, $\beta_v(f)$ can be described by three parameters, the effective mode index, n_{eff} , the group mode index, n_{gr} and the group velocity dispersion D_v , each resolved at some reference frequency f_0 .

Active components were modelled using time-domain modelling and controlled by constant, or time-dependent electrical signal blocks that represented applied oscillating voltages or direct current sources. The 1 mm long EOPMs were characterised by a non-linear, function-driven, voltage-dependent phase shift, such that the behaviour closely matched the foundry design manual. SOA blocks were defined by a parabolic gain shape model with user defined central

wavelength, bandwidth and peak gain parameters according to the foundry specifications. The model provided optimal input criteria of variable optical and electrical driving inputs as well as the tolerance to deviation from these optimal conditions.

The conditions highlighted in Eq. (1) and Eq. (2) identified critical assignment of both ω_0 and ω_m such that they are in resonance with ω_{loop} . To determine ω_{loop} , a simple passive loop constructed of 12 mm of passive waveguide and a 2x2 coupler was modelled. An optical input was swept over a short wavelength range near 1550 nm. By measuring the power output, the frequency dependent resonance peaks were observed with a separation of 6.61 GHz. Both ω_m and ω_0 were then assigned such that Eq. (1) and Eq. (2) were satisfied, with ω_0 selected as the nearest integer harmonic to 193.4 THz to generate comb spectra as in Fig. 2(a).

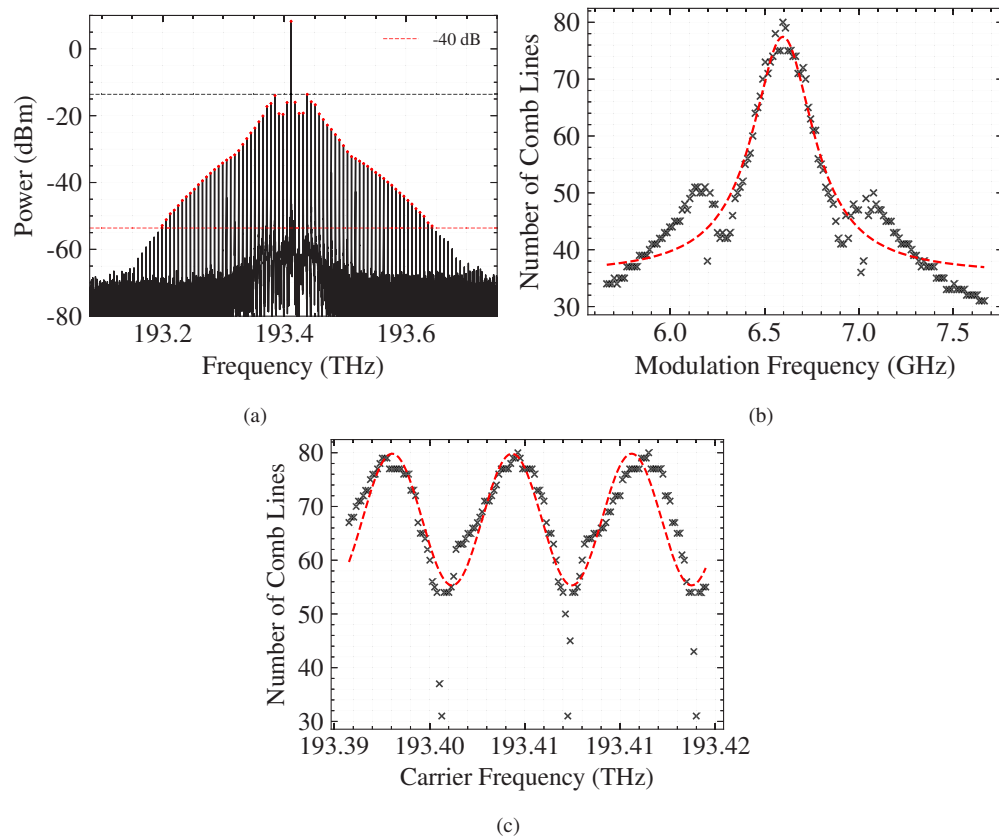


Fig. 2. (a) Comb spectrum generated from the photonic circuit model (black), with comb line peaks highlighted in red, (b) Detuning behaviour of ω_m on the number of comb lines in each spectra (black). A curve fit (red) denotes a peak at 6.60 GHz and a detuning range of ± 170 MHz to sustain comb spectra with >60 comb lines. (c) Detuning effect of ω_0 . A sine curve was fit (red), highlighting the periodicity of resonant conditions with a detuning range of ± 2.7 GHz was capable of generating combs with >60 comb lines

The effect of detuning the modulation frequency from the resonance conditions was assessed by generating many comb spectra for a sweep of applied ω_m over a 2 GHz range centred about the resonant loop frequency of 6.61 GHz and determining the number of comb lines. Broad comb spans were observed when ω_m was equal to 6.60 GHz, which closely matched the modelled loop resonance. Figure 2(b) shows the generation of 80 comb lines within a 40 dB power envelope that spans 528 GHz at optimal resonant conditions. As ω_m was detuned from ω_{loop} , the number

of comb lines sharply reduced. A best fit curve was plotted identifying a narrow span in which a large number of comb lines were generated. From this curve, an offset detuning range for the modulation frequency was quantified as the frequency offset from the peak modulation frequency that sustained comb spectra with >60 comb lines within a 40 dB power envelope power envelope. The offset detuning range was found to be ± 170 MHz, requiring ω_m to be accurately assigned within this limit to ensure broad comb spans are achieved. Small off-resonant peaks were observed at ± 500 MHz from the resonant modulation frequency of 6.60 GHz. For these instances the comb spectra exhibited highly asymmetric comb line distributions where a higher number of comb lines were present on one side of the carrier frequency. For modulation frequencies below the loop resonance, asymmetric comb spectra were generated with more comb lines at lower frequencies with respect to the carrier frequency. Conversely, modulation frequencies above ω_{loop} generated asymmetric distributions with a larger number of comb lines at higher frequencies compared to the carrier frequency.

A similar investigation into the effect of non-resonant behaviour was performed on ω_0 with ω_m set optimally at 6.60 GHz. A sweep of ω_0 between 193.395 THz and 193.415 THz was performed to demonstrate the effect on the total number of comb lines in each spectra. Depicted in Fig. 2(c), periodic behaviour was observed with a maximum of 80 comb lines within a 40 dB power envelope generated when ω_0 was resonant with the ω_{loop} and a minimum of 31 comb lines when off resonance. The periodicity was quantified by a sine function best fit with a frequency of ~ 6.30 GHz demonstrating a similar frequency to the modelled loop resonance and highlighting the capability for tuning the carrier frequency in frequency steps that are harmonic with the round-trip loop frequency. Through the evaluation of a single peak, the detuning range for ω_0 to sustain >60 comb lines within a 40 dB power envelope was found to be ± 2.7 GHz.

4. Photonic integrated device

4.1. Fabrication and assembly

The InP PIC was fabricated as part of a multi-project wafer run using generic foundry methods. Contained within the 6 x 2 mm² PIC footprint (depicted in Fig. 3) were multiple iterations of the integrated comb generator design. The 2 highlighted loops (Loop_01 in red and Loop_02 blue) shared a similar architecture but operated at different round-trip loop frequencies due to the difference in loop lengths. In the following description of the experimental setup, Loop_01, with a loop length of 12 mm is evaluated unless otherwise stated.

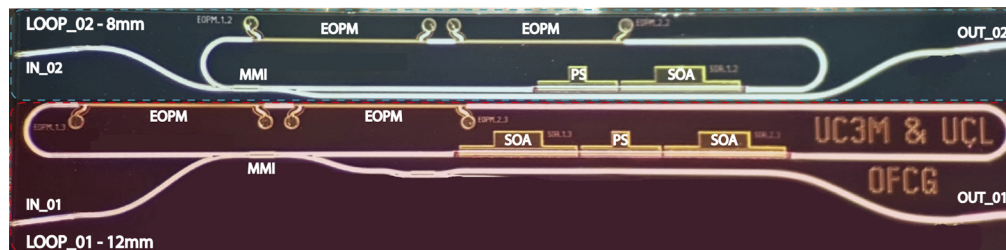


Fig. 3. Optical microscope image of the fabricated PIC with the 2 separate OFCG looped structures indicated in Red (Loop_01) and Blue (Loop_02) that occupy a PIC area of ~ 1.3 mm x 6 mm. With components IN/OUT: spot-size converter facets, MMI: multimode interference coupler, PS: phase shifter, SOA: semiconductor optical amplifier, EOPM: electro-optic phase modulator

The input and output facets were defined by vertically tapered waveguide spot-size converters (SSCs) which optimised the coupling efficiency and allowed lensed fibres to be edge-coupled to the PIC with coupling losses of around 5-6 dB. The SSCs were angled at a 7° offset with respect

to the facet normal which, alongside a 22° offset of the lensed fibre and an anti-reflective coating applied to the facet surface minimised the effect of back-reflections at the coupling interfaces. Optical isolators with 40 dB isolation were included at both input and output fibres to further reduce back-reflections. Both the passive and active waveguide components were optimised for transverse electric (TE) polarisation, therefore an appropriate polarisation controller was included at the coupled optical input.

Input and output waveguides were coupled to the amplified recirculating loop structure by a 2×2 multimode interference (MMI) coupler with a 50:50 splitting ratio. Though this splitting ratio was unlikely to achieve an optimal coupling efficiency [25], alternative splitting ratios were unavailable in the process design kit (PDK). The excess loss of the MMI coupler was expected to be 0.25 dB. The loop was comprised of deep-etched passive waveguides that contributed around 6 dB/cm of propagation losses. For Loop_01 this accounted for approximately 7.2 dB losses per recirculation, with waveguide sections that extended to and from the loop and the PIC edges contributing a further 3.9 dB loss. The bend radii of the passive waveguides was $150 \mu\text{m}$ and contributed negligible additional losses.

Two 1 mm long multi-quantum-well (MQW) electro-absorption modulators were cascaded and embedded within the loop, exhibiting ~ 7 dB insertion loss at 1550 nm. A reverse bias was applied to induce phase modulation behaviour through the quantum confined Stark effect (QCSE). SOA components with active MQW waveguides provided amplification within the loop when driven with a direct current (DC). Due to the increased length of Loop_01, a secondary SOA component was included opposed to the single SOA in Loop_02. This ensured the increased propagation losses accumulated by the loop could be compensated for. Short phase shifter (PS) sections were included within the loop that provided the capability to tune the refractive index over a small range by direct current injection.

The InP PIC was mounted alongside alumina interposers to an aluminium nitride subassembly. Electrical connections from the PIC were wire bonded to the interposers which contained a combination of grounded coplanar waveguides (G-CPWs) for RF connections, and DC signal lines. The G-CPWs were designed with dimensions to operate at 50Ω impedance. RF connections were further extended with wirebonds from the interposer to a pitch increasing, high frequency printed circuit board (PCB) with multiple SMA RF port connectors. Each EOPM was connected to two RF ports where one provided the reverse-biased RF drive signal through a bias tee and the other was terminated at 50Ω . DC current was provided to each of the SOAs and PS sections directly via the interposer. The subassembly was then mounted to a copper heatsink block which was grounded, and thermally stabilised at 20°C by a thermo-electric cooler (TEC).

4.2. Component characterisation

Characterisation of the SOAs was performed directly on the components situated within the loop. For a range of bias currents between 30 mA - 150 mA, the small signal gain as a function of wavelength was measured on a high-resolution (10 MHz) optical spectrum analyser (OSA) as seen in Fig. 4(a). This demonstrated an ASE noise floor of -75 dBm with an increasing gain and 3 dB optical bandwidth as the injection current is increased. When the injection current surpassed ~ 75 mA the typical parabolic SOA gain profile is distorted at around 1580 nm which may increase asymmetry behaviour in the comb spectra. Therefore, to correctly operate the SOA components within the amplified recirculating loop the current was set below this limit demonstrating a maximum gain recorded at 75 mA of around 14.5 dB with a peak at 1535 nm and a 3 dB optical bandwidth of 45 nm.

The phase modulators were characterised from identical components integrated separately to the OFCG system and configured in the parallel, dual branch layout of a MZM. The electrical connections were similarly terminated in 50Ω . The output optical power was measured for increasing reverse bias on one branch of the MZM to record a transfer function for the device

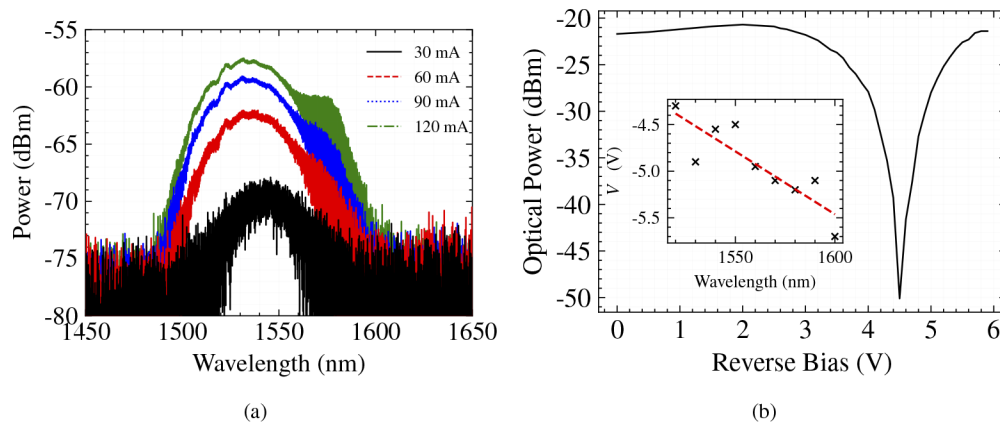


Fig. 4. (a) ASE spectra of the SOA when injected with increasing currents. Small injection currents yielded low gain and narrow 3 dB bandwidths. However, injection currents beyond 90 mA (blue and green) resulted in a distortion of the parabolic SOA gain profile at around 1580 nm. (b) Transfer function of the characterised MZM at 1550 nm with a V_{π} of 4.5 V. The inset shows the change in V_{π} as a function of wavelength

at 1550 nm which is shown in Fig. 4(b). Here, the extinction ratio can be identified as 28 dB and the V_{π} was measured at around 4.5 V. Over a range of wavelengths between 1520 nm and 1600 nm, the V_{π} was demonstrated (inset of Fig. 4(b)) to remain within a 1 V window of that measured at 1550 nm with extinction ratios >20 dB.

4.3. Experimental setup

The optical input was supplied by a tunable external cavity CW laser source with a linewidth of 100 kHz and power set at 10 dBm to avoid gain saturation of the SOA components. The wavelength was set to 1550 nm, then tuned to the nearest integer harmonic of the round-trip loop frequency.

The modulation frequency was provided by an externally referenced Rohde and Schwarz SMF100A signal generator outputting 15 dBm power. The signal was split by an appropriate bandwidth RF splitter to allow synchronous modulation to each of the EOPMs via RF phase shifter delay lines which provided precise control of the phase alignment to phase match the electrical drive supplied to the EOPMs. After accounting for losses in the splitter and phase shifters, it was necessary to amplify the RF signal with low noise RF amplifiers that boosted the power to around 24 dBm ($V_{pp} \sim 10$ V) per channel. Each amplified RF signal was provided with a reverse bias of 7 V via bias tee components which was found to generate the largest number of comb lines, and was delivered to ports on the PCB corresponding to the EOPMs on PIC.

SOA and PS sections were controlled by a Thorlabs PRO8000 current control. SOA_{01} was driven at transparency with around 12.5 mA, whilst SOA_{02} was driven with around 65 mA providing sufficient gain to compensate for the loop losses. The PS section was provided with small injection currents of <2.5 mA and used to perform finely tuned optimisation of the loop length.

To generate the comb, both the carrier frequency and the modulation frequency were set to resonant conditions of the loop. Fine adjustment of the electrical and optical phase shifters was then performed to fully optimise the spectrum enabling the maximum comb spans to be achieved. The optical output was measured on an OSA with 10 MHz resolution. RF spectra and phase noise measurements were recorded by outputting the comb to a high-speed photodiode and measuring

the electrical response of the beat note frequencies on an Rohde and Schwarz FSU Spectrum Analyzer.

5. Experimental results

5.1. Comb generation

Firstly, the round-trip loop frequency was measured for Loop_01 by driving the SOAs at transparency and injecting the loop with a constant power optical signal that swept over a range of wavelengths close to 1550 nm. Figure 5(a) shows the measured periodic optical output that peaked when the input frequency was resonant with the cavity modes of the loop, where the peaks were evenly spaced with a separation equal to the round-trip loop frequency. Using a sine fitting function, an accurate FSR was interpreted as 6.80 GHz for the 12 mm length loop. This indicated that the round-trip loop frequency was in line with, but slightly higher than predicted in the model in Section 3. and was likely a consequence of fabrication tolerances. Although this comb generation technique is not reliant on a high Q-factor cavity to enable broad comb generation, the Q-factor of the passive loop was calculated from the transmission frequency and corresponding full-width half maximum in Fig. 5(a) to be 50×10^3 .

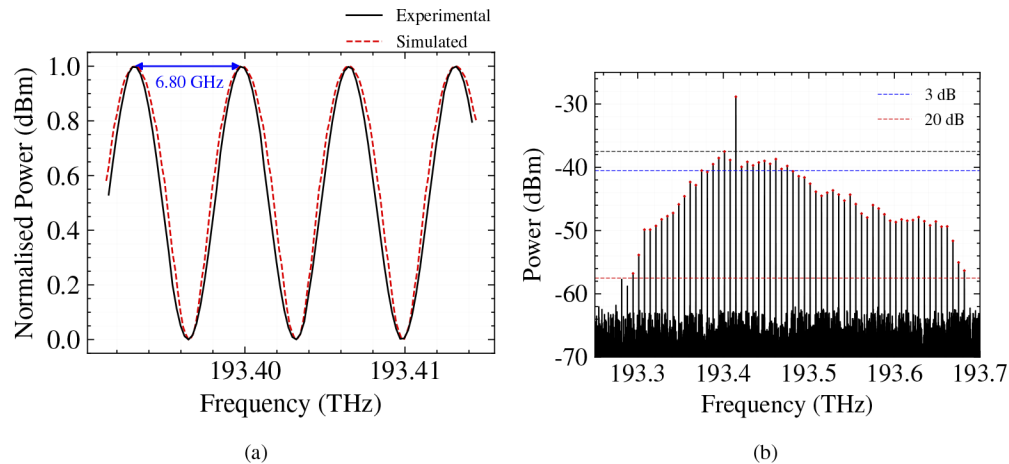


Fig. 5. (a) Loop resonance was measured experimentally (black) demonstrating a round-trip loop frequency of 6.80 GHz whilst the simulated model resulted in a 6.61 GHz separation (red), (b) Optical spectrum generated by the device on an OSA with resolution bandwidth of 10 MHz. Red crosses identify peaks contained within a 20 dB power envelope that excludes the carrier frequency

The maximum number of comb lines was observed when the applied modulation frequency equalled 6.71 GHz, deviating from the measured round-trip loop frequency due to the application of a small injection current to the phase shifter section of ~ 0.5 mA as part of the fine-tuning optimisation. The comb spectrum of Loop_01 can be seen in Fig. 5(b). generating a total of 59 comb lines within a 20 dB power envelope that excluded the carrier frequency and expanded over approximately a 400 GHz span. The narrower comb span observed experimentally compared to the simulated comb in Section 3 was likely attributed to increased dispersion effects in the waveguide. Although a dispersion parameter was included in the simulation, the simplified group velocity dispersion parameter may not have been a sufficient representation of the full waveguide dispersion that was experienced in the experimental devices thus narrower comb bandwidths were generated. Furthermore, the comb displayed an asymmetric appearance, suggesting ω_m was not fully resonant with the round-trip loop frequency despite fine-tuning optimisation with the

phase shifter. The flatness of the comb is summarised in Table 2, where the number of comb lines encompassed within reducing power envelopes drops to a minimum of 14 comb lines within a 3 dB power deviation. This amounts to a 3 dB bandwidth of 94 GHz.

Table 2. Number of Comb Lines Generated within Specified Power Envelope

FSR	3 dB	5 dB	10 dB	20 dB
6.71GHz	14	20	37	59

A significant feature of the comb spectrum was the prominent comb line at the seed laser frequency, presenting with a power difference of ~ 10 dBm greater than adjacent peaks. This was a consequence of using a 50:50 splitting ratio for the MMI coupler that injected the seed laser into the loop which allowed half of the input optical power to bypass the loop and propagate directly through the PIC without experiencing modulation from the embedded phase modulators, resulting in an increased power output for the carrier frequency. The average power output for the remaining comb lines was around -45 dBm, equating to an optical carrier-to-noise ratio (OCNR) of 20 dB when compared to the -65 dBm noise floor measured with a 10 MHz resolution bandwidth. The splitting ratio of 50:50 alongside poor coupling efficiency of the fibre coupled output contributed to a low power conversion efficiency of the device.

The electrical spectrum of the comb was measured on a high-speed photodiode, which demonstrated strong and distinct peaks at integer harmonics of the comb line spacing (Fig. 6(a)). Due to limitations in bandwidth of the measurement equipment, the first 3 peaks were observed. The inset in Fig. 6(a) depicts a zoomed perspective of the 6.71 GHz peak within a 50 MHz window, where the narrow peak observed demonstrates strong phase coherence of the generated comb lines. Composite amplitude and phase noise measurements were performed on the unfiltered comb spectrum for each of the 3 observed beat notes as shown in Fig. 6(b). The inference of strong phase coherence was reinforced from low phase noise characteristics at 100 kHz offset, with the 6.71 GHz beat note demonstrating a phase noise as low as -105 dBc/Hz. Each of the 3 beat notes displayed a low phase noise measurement of < -75 dBc/Hz at the minimum frequency offset limit of 100 Hz and for each increasing integer harmonic measured, the phase noise increased by approximately 6 dB at 100 kHz.

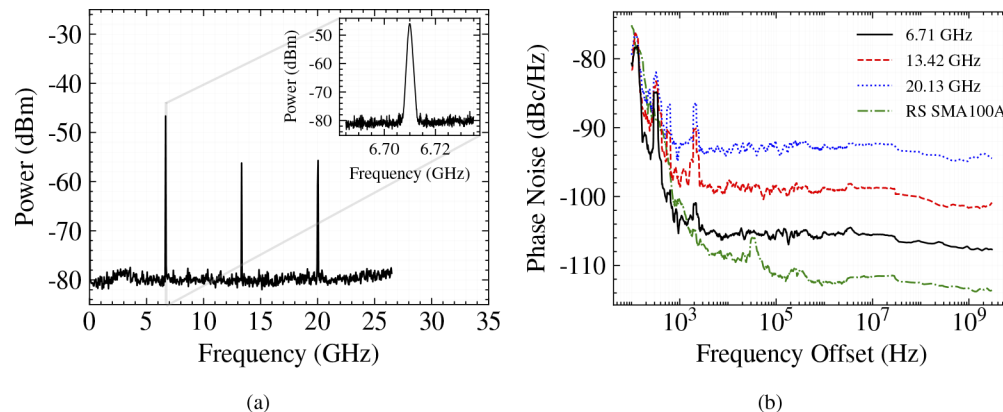


Fig. 6. (a) The electrical spectrum of the comb from a high-speed photodiode measured with a resolution bandwidth of 3 MHz, demonstrating defined peaks at multiples of the FSR. The inset shows a 50 MHz span about the first peak with a resolution bandwidth of 500 kHz (b) the phase noise measured for the first three beat notes including the noise floor of the RF synthesiser (RS SMA100A)

5.2. Tunability

Due to the fixed loop length of the system and the associated round-trip loop frequency, the comb line spacing of the amplified recirculating loop OFCG is coarsely locked depending upon the fabricated design. Therefore to attain specific FSRs, devices must be designed and fabricated with different loop lengths. To demonstrate the effect of different loop lengths on the FSR, another device, labelled Loop_02 in Fig. 3 was fabricated with a similar architecture to the fully characterised 12 mm long device (Loop_01). The second device was configured with an 8 mm long loop, accommodating a round-trip loop frequency of approximately 10 GHz. Using the same experimental process, a comb was generated for the second loop that consisted of 57 comb lines within a 20 dB power envelope, where the comb lines were evenly spaced by 10.1 GHz to cover a total span of ~570 GHz (Fig. 7(a)).

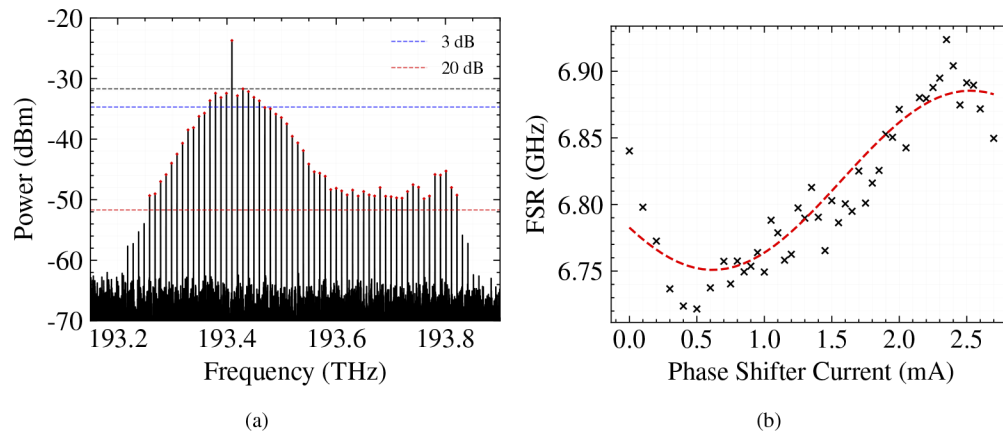


Fig. 7. (a) Optical spectrum (resolution bandwidth: 10 MHz) of device operating at 10.1 GHz FSR, generating 57 comb lines over a span of ~570 GHz. Red crosses identify peaks contained within a 20 dB power envelope that excludes the carrier frequency (b) The measured FSR (black) for comb spectra at increasing injection currents applied to the phase shifter section of the 6.71 GHz loop. A polynomial fit (red) highlights an effective tuning range of the FSR of approximately 150 MHz

Although large changes in the FSR required different loop lengths, some tunability of the FSR was achieved by the inclusion of phase shifter components embedded within the loop. Small injection currents applied to the phase shifter sections induced changes to the refractive index of the waveguide, effectively altering the length of the loop. Loop resonance measurements were recorded as in Fig. 5(a) for a range of injection currents up to 2.5 mA and collated in Fig. 7(b) to demonstrate the capability to tune the otherwise static 6.8 GHz loop length over a tuning range of 150 MHz of the FSR. This tunability enabled optimisation of the overlap of the cavity mode and the driving modulation frequency to better meet the conditions for optimal comb generation as well as providing the potential to expand the comb span by up to 8.8 GHz.

6. Conclusions

In this work, a novel integrated optical frequency comb generation technique was demonstrated, utilising linearly cascaded modulators embedded within an amplified recirculating loop. Simulations were used to identify tolerance limitations for the applied modulation frequency and seed laser frequency, enabling optimal conditions to be satisfied for broad comb span generation. Two separate devices were measured experimentally with combs operating with FSRs of 6.71 GHz and 10.1 GHz and spanning a total of ~400 GHz and ~570 GHz respectively. Flatness of

the spectra was highlighted through 3-dB bandwidths of 94 GHz for the 6.71 GHz loop and 111 GHz for the 10.1 GHz loop. Strong phase coherence between comb lines was indicated by phase noise measurements of -105 dBc/Hz at 100 kHz. Though many of the benefits of EO based comb generators were preserved using our technique, the flexibility of coarse FSR tunability is lost through the limitations of the fixed length of waveguide that comprised the loop. However, through the inclusion of a short phase shifter component within the loop, some FSR tunability was restored to provide a small tuning range of up to 150 MHz. The recirculating loop enabled an efficient use of a low number of active integrated components when compared to similar EO-based OFCGs on InP with many cascaded modulators [21], reducing the complexity of driving electronics and therefore the overall power consumption of the device whilst maintaining a compact footprint and generating a larger number of comb lines. These characteristics, alongside promising comb spectra results identify the integrated amplified recirculating loop technique of OFCG demonstrated in this work as a potential solution for implementation in SWaP-dependent applications such as satellite payloads and on-board automotive systems.

Funding. Engineering and Physical Sciences Research Council (EP/L015455/1, EP/P021859/1, EP/S000976/1).

Acknowledgments. This research work has been supported by the UK Engineering and Physical Sciences Research Council (EPSRC) through the Integrated Photonics and Electronic Systems (IPES) Centre of Doctoral Training and PICSat project (EPSRC Reference: EP/S000976/1).

Disclosures. The authors declare no conflicts of interest.

Data availability. Data underlying the results presented in this paper are not publicly available at this time but may be obtained from the authors upon reasonable request.

References

1. J. Ye, H. Schnatz, and L. W. Hollberg, "Optical frequency combs: From frequency metrology to optical phase control," *IEEE J. Sel. Top. Quantum Electron.* **9**(4), 1041–1058 (2003).
2. K. Balakier, M. J. Fice, L. Ponnampalam, A. J. Seeds, and C. C. Renaud, "Monolithically integrated optical phase lock loop for microwave photonics," *J. Lightwave Technol.* **32**(20), 3893–3900 (2014).
3. N. Picqué and T. W. Hänsch, "Frequency comb spectroscopy," *Nat. Photonics* **13**(3), 146–157 (2019).
4. R. I. Hermans, J. Seddon, H. Shams, L. Ponnampalam, A. J. Seeds, and G. Aeppli, "Ultra-high-resolution software-defined photonic terahertz spectroscopy," *Optica* **7**(10), 1445 (2020).
5. N. Kuse and M. E. Fermann, "Frequency-modulated comb lidar," *APL Photonics* **4**(10), 106105 (2019).
6. H. Hu and L. K. Oxenløwe, "Chip-based optical frequency combs for high-capacity optical communications," *Nanophotonics* **10**(5), 1367–1385 (2021).
7. P. Marin-Palomo, J. N. Kemal, T. J. Kippenberg, W. Freude, S. Randel, and C. Koos, "Performance of chip-scale optical frequency comb generators in coherent wdm communications," *Opt. Express* **28**(9), 12897 (2020).
8. R. Liao, H. Tian, W. Liu, R. Li, Y. Song, and M. Hu, "Dual-comb generation from a single laser source: Principles and spectroscopic applications towards mid-IR—a review," *JPhys Photonics* **2**(4), 042006 (2020).
9. X. Yang, K. Xu, J. Yin, Y. Dai, F. Yin, J. Li, H. Lu, T. Liu, and Y. Ji, "Optical frequency comb based multi-band microwave frequency conversion for satellite applications," *Opt. Express* **22**(1), 869–877 (2014).
10. J. Anzalchi, P. Inigo, and B. Roy, "Application of photonics in next generation telecommunication satellites payloads," *Proc. SPIE* **10563**, 140 (2017).
11. M. Ruiz-Llata, M. A. Lombana, O. E. Bonilla-Manrique, and P. Acedo, "Pavement condition sensor based on a dual optical frequency comb generator," *Opt. Lasers Eng.* **158**, 107172 (2022).
12. S. Liu, X. Wu, D. Jung, J. C. Norman, M. J. Kennedy, H. K. Tsang, A. C. Gossard, and J. E. Bowers, "High-channel-count 20ghz passively mode-locked quantum dot laser directly grown on si with 4.1 tbit/s transmission capacity," *Optica* **6**(2), 128–134 (2019).
13. Z. Lu, J. Liu, S. Raymond, P. Poole, P. Barrios, and D. Poitras, "312-fs pulse generation from a passive c-band inas/inp quantum dot mode-locked laser," *Opt. Express* **16**(14), 10835–10840 (2008).
14. M.-C. Lo, R. Guzmán, and G. Carpintero, "Inp femtosecond mode-locked laser in a compound feedback cavity with a switchable repetition rate," *Opt. Lett.* **43**(3), 507–510 (2018).
15. M. L. Davenport, S. Liu, and J. E. Bowers, "Integrated heterogeneous silicon/iii-v mode-locked lasers," *Photonics Res.* **6**(5), 468 (2018).
16. E. Vissers, S. Poelman, C. O. de Beeck, K. V. Gasse, and B. Kuyken, "Hybrid integrated mode-locked laser diodes with a silicon nitride extended cavity," *Opt. Express* **29**(10), 15013 (2021).
17. M. D. G. Pascual, V. Vujicic, J. Braddell, F. Smyth, P. Anandarajah, and L. Barry, "Photonic integrated gain switched optical frequency comb for spectrally efficient optical transmission systems," *IEEE Photonics J.* **9**(3), 1–8 (2017).
18. M. D. G. Pascual, V. Vujicic, J. Braddell, F. Smyth, P. M. Anandarajah, and L. P. Barry, "Inp photonic integrated externally injected gain switched optical frequency comb," *Opt. Lett.* **42**(3), 555–558 (2017).

19. R. Slavík, S. G. Farwell, M. J. Wale, and D. J. Richardson, "Compact optical comb generator using inp tunable laser and push-pull modulator," *IEEE Photonics Technol. Lett.* **27**(2), 217–220 (2015).
20. N. Andriolli, T. Cassese, M. Chiesa, C. de Dios, and G. Contestabile, "Photonic integrated fully tunable comb generator cascading optical modulators," *J. Lightwave Technol.* **36**(23), 5685–5689 (2018).
21. F. Bontempi, N. Andriolli, F. Scotti, M. Chiesa, and G. Contestabile, "Comb line multiplication in an inp integrated photonic circuit based on cascaded modulators," *IEEE J. Sel. Top. Quantum Electron.* **25**(6), 1–7 (2019).
22. Z. Wang, M. Ma, H. Sun, M. Khalil, R. Adams, K. Yim, X. Jin, and L. R. Chen, "Optical frequency comb generation using cmos compatible cascaded mach-zehnder modulators," *IEEE J. Quantum Electron.* **55**(6), 1–6 (2019).
23. T. Ren, M. Zhang, C. Wang, L. Shao, C. Reimer, Y. Zhang, O. King, R. Esman, T. Cullen, and M. Lončar, "An integrated low-voltage broadband lithium niobate phase modulator," *IEEE Photonics Technol. Lett.* **31**(11), 889–892 (2019).
24. M. Xu, M. He, Y. Zhu, S. Yu, and X. Cai, "Flat optical frequency comb generator based on integrated lithium niobate modulators," *J. Lightwave Technol.* **40**(2), 339–345 (2022).
25. M. Zhang, B. Buscaino, C. Wang, A. Shams-Ansari, C. Reimer, R. Zhu, J. M. Kahn, and M. Loncar, "Broadband electro-optic frequency comb generation in a lithium niobate microring resonator," *Nature* **568**(7752), 373–377 (2019).
26. L. Chang, S. Liu, and J. E. Bowers, "Integrated optical frequency comb technologies," *Nat. Photonics* **16**(2), 95–108 (2022).
27. H. Sun, M. Khalil, Z. Wang, and L. R. Chen, "Recent progress in integrated electro-optic frequency comb generation," *J. Semicond.* **42**(4), 041301 (2021).
28. A. Parriaux, K. Hammani, and G. Millot, "Electro-optic frequency combs," *Adv. Opt. Photonics* **12**(1), 223 (2020).
29. K. P. Ho and J. M. Kahn, "Optical frequency comb generator using phase modulation in amplified circulating loop," *IEEE Photonics Technol. Lett.* **5**(6), 721–725 (1993).
30. S. Bennett, B. Cai, E. Burr, O. Gough, and A. J. Seeds, "1.8-thz bandwidth, zero-frequency error, tunable optical comb generator for dwdm applications," *IEEE Photonics Technol. Lett.* **11**(5), 551–553 (1999).
31. L. Ponnampalam, M. Fice, H. Shams, C. Renaud, and A. Seeds, "Optical comb for generation of a continuously tunable coherent thz signal from 1225 ghz to >2.7thz," *Opt. Lett.* **43**(11), 2507 (2018).
32. P. Shen, N. J. Gomes, P. A. Davies, P. G. Huggard, and B. N. Ellison, "Analysis and demonstration of a fast tunable fiber-ring-based optical frequency comb generator," *J. Lightwave Technol.* **25**(11), 3257–3264 (2007).
33. X. Wang and S. Mookherjea, "Performance comparisons between semiconductor and fiber amplifier gain assistance in a recirculating frequency shifter," *Opt. Lett.* **43**(5), 1011–1014 (2018).